Appl. Phys. B 84, 683–690 (2006)
DOI: 10.1007/s00340-006-2396-6

Applied Physics B
Lasers and Optics

Design of the cold atom PHARAO space clock and initial test results

PH. LAURENT[1]
M. ABGRALL[4]
CH. JENTSCH[1]
P. LEMONDE[1]
G. SANTARELLI[1]
A. CLAIRON[1]
I. MAKSIMOVIC[1]
S. BIZE[1]
CH. SALOMON[3,✉]
D. BLONDE[2]
J.F. VEGA[2]
O. GROSJEAN[2]
F. PICARD[2]
M. SACCOCCIO[2]
M. CHAUBET[2]
N. LADIETTE[2]
L. GUILLET[2]
I. ZENONE[2]
CH. DELAROCHE[2]
CH. SIRMAIN[2]

[1] SYRTE, 61 avenue de l'Observatoire, 75014 Paris, France
[2] CNES, 18 avenue Edouard Belin, 31401 Toulouse cedex, France
[3] Laboratoire Kastler Brossel, 24 rue Lhomond, 75231 Paris, France
[4] ALTEN, Prologue BP 27-04, 31312 Labege, France

Received: 16 June 2006/Revised version: 23 June 2006
Published online: 31 August 2006 •

ABSTRACT In this paper we describe the cold atom clock PHARAO, designed for microgravity operation. All elements of the PHARAO engineering model have been manufactured and delivered to CNES, the French space agency. We present the clock design, its main characteristics, and initial science operation. PHARAO is one of the main components of the Atomic Clock Ensemble in Space payload that is scheduled to fly on board the International Space Station in 2010.

PACS 07.87.+v; 06.30.Ft; 95.55.Sh; 32.80.Pj

1 Introduction

The PHARAO[1] cold atom clock is one of the two atomic clocks of the space mission ACES[2] [1] managed by the European Space Agency ESA. In addition to this clock, the ACES payload includes a hydrogen maser (H maser) developed by the Observatoire Cantonal de Neûchatel (Switzerland), a phase/frequency comparator and signal distribution package, as well as a two-way time-transfer link developed by Timetech/Kaiser-Threde/EADS-ST (Germany). The H maser, thanks to its good medium-term frequency stability (10^{-15} over 1 h), serves as a reference oscillator for the PHARAO clock performance evaluation and time keeping for durations below 1 h. The ACES mission is scheduled to fly on board the International Space Station for a duration of at least 18 months. Science objectives of ACES include the study of the PHARAO cesium clock in microgravity, time and frequency comparisons with ultra-stable Earth-based clocks, search for drift of fundamental constants, and a measurement of the Einstein effect (red shift) with a 2 ppm uncertainty.

The expected frequency stability of the PHARAO clock in space is $10^{-13}\ \tau^{-1/2}$, where τ is the integration time in seconds and the target accuracy is 10^{-16}. The stability of the time-comparison system is better than 6 ps/day.

The French space agency CNES is funding and acting as the prime contractor of the PHARAO clock, which was designed by SYRTE, LKB, and CNES building upon several years of experience with cold atom fountain frequency standards using cesium and rubidium atoms. The clock industrial development began in 2002 by the realization of an engineering model representative of the flight model in terms of interfaces, design, and full functionality. The current PHARAO budgets in mass, volume, power dissipation, and data-transfer rate are 91 kg, 200 l, 88 W, and 87 Mbytes/day, respectively. As a cold atom clock includes several state-of-the art technologies, the PHARAO instrument has been divided into four sub-systems which are procured from different manufacturers.

Figure 1 shows the clock architecture. The laser source provides 14 laser beams through 10 optical fibers to manipulate and probe the cesium atoms in a UHV vacuum chamber, the cesium tube. Both systems have been developed by EADS-SODERN. In the cesium tube, atoms are captured, cooled, prepared in a magnetic sub-state, excited by the 9.2-GHz interrogation microwave field, and finally detected by laser-induced fluorescence (Fig. 2). The microwave source developed by TAS, based on a 5-MHz ultra-stable quartz oscillator from CMAC, feeds the 9.2-GHz signal to the preparation and interrogation microwave cavities. A 100-MHz signal is sent from PHARAO to the ACES com-

✉ Fax: +33-1-44-32-34-34, E-mail: christophe.salomon@lkb.ens.fr
[1] Projet d'Horloge Atomique à Refroidissement d'Atomes en Orbite
[2] Atomic Clock Ensemble in Space

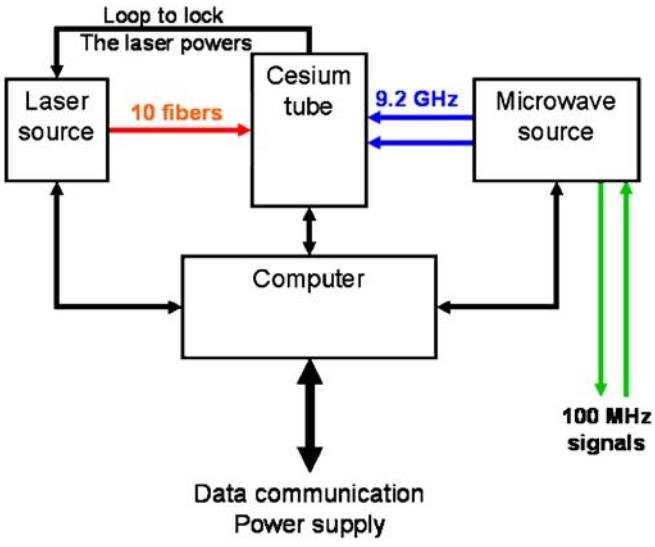

FIGURE 1 Diagram of the PHARAO clock architecture. The four subsystems have been independently developed by industrial companies. The *black lines* represent the electrical connections. The power of each laser beam at the fiber's output is monitored by a photodiode and actively stabilized by the servo loop

parator for phase comparisons with the H maser. Finally, a computer (developed by EREMS) with dedicated software (developed by CSSI) manages the clock operation and the data communications.

2 The laser source

The laser source architecture is shown in Fig. 3. An extended cavity diode laser (ECDL) is locked to the saturated absorption crossover resonance of cesium ($6S_{1/2}$, $F = 4 \rightarrow 6P_{3/2}$, $F = 4/F = 5$) through an acousto-optic modulator (AOM1). This new ECDL design has an intra-cavity etalon for rugged and reliable behavior [2, 3]. To perform the frequency locking, the diode laser current is modulated at 500 kHz and the absorption signal is synchronously demodulated to provide the error signal. This signal is applied to the diode laser current and to the PZT transducer that drives the cavity length of the ECDL. The measured frequency noise level reaches 10^4 Hz^2/Hz at a Fourier frequency of 100 Hz. By changing the AOM1 rf frequency the laser frequency can be tuned over 80 MHz with a rate of 260 kHz/μs. This ECDL/AOM combination provides the frequency reference for all the atom processes: capture, cooling, selection, and detection.

A second ECDL is used as a redundant laser source. Its beam is superimposed onto the first by means of a polarizing cube. When used, its polarization is turned by 90° by moving a half-wave retardation plate mounted on a bistable motorization. The master laser beam goes through a 30-dB optical isolator. Its power is 30 mW for a diode laser current of 70 mA. As the AOM1 is in the frequency loop, the main laser beam alignment is not perturbed by the frequency tuning. The beam is then split into three beams. One beam is coupled into two optical fibers through an acousto-optic modulator (AOM2). It is used for the atomic detection (10 mW) and selection (5 mW) and the laser power is adjusted and controlled by the AOM2 rf power. The resolution is 10 μW with a dynamic range of about 25 dB. This AOM2 operates at a frequency of 75 MHz. The second part of the beam double passes through an acousto-optic modulator (AOM3) before injecting a slave diode laser. The AOM3 frequency can be adjusted from 90 MHz to 86 MHz to launch atoms (from 5 cm/s to 5 m/s) with the moving molasses method [4]. The third beam injection locks a second slave diode laser. Each slave laser also has a redundant diode laser. The slave diode lasers remain locked over a 2-mA current variation. A photodiode behind a cesium cell is used to check the injection. After an optical isolator, the slave laser beam passes through a 90-MHz acousto-optic modulator (AOM4) and is divided into three beams. The two slave lasers then provide the six beams (3 + 3 counterpropagating) to make the optical molasses geometry. The AOM4 rf power determines the capture and cooling intensities, which can be decreased with a slew rate of 40 dB over 300 μs to perform adiabatic cooling after launch of the atoms. Each beam is reflected by a mirror mounted on four PZT transducers (Cedrat). This allows a fine alignment

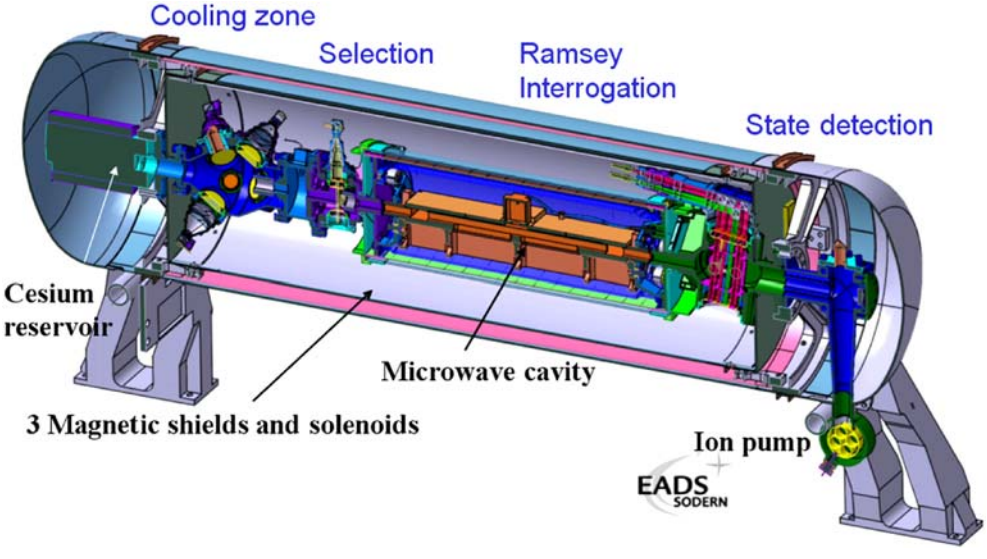

FIGURE 2 Cross section of the PHARAO clock tube. Atoms from a cesium vapor are captured in the cooling zone. After launch and selection into a well-defined magnetic sub-state, the atoms interact with a microwave field in the two active sections of a 20-cm-long Ramsey cavity. The atoms in both hyperfine levels are detected downstream by laser-induced fluorescence. The overall length of the device is 990 mm

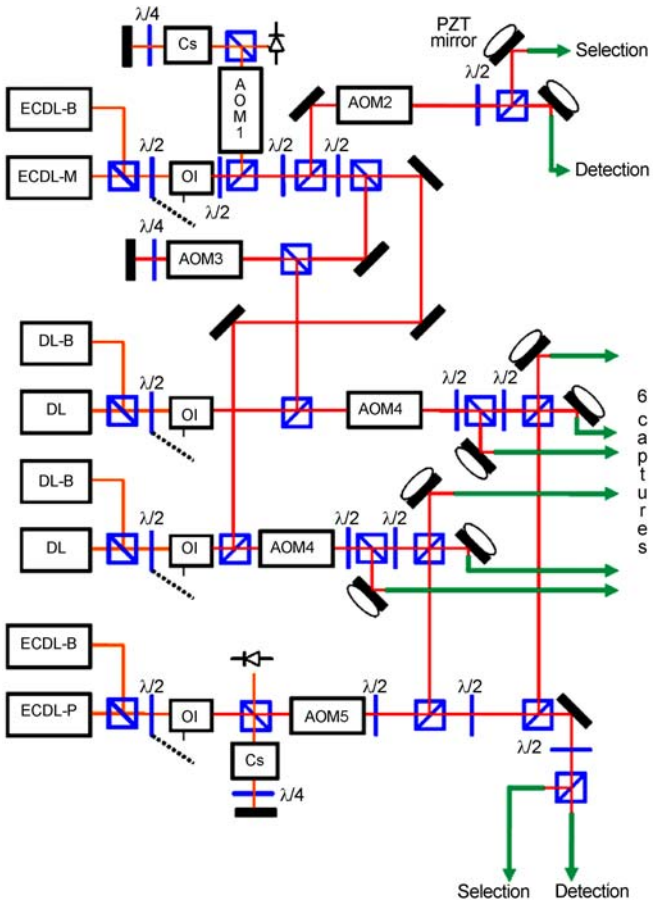

FIGURE 3 Optical architecture of the laser source. The five mechanical shutters are not represented. The optical fibers are indicated by the *green outgoing arrows*. ECDL: extended cavity diode laser (M: master, P: pump, B: backup). DL: diode laser, AOM: acousto-optic modulator, OI: optical isolator, Cs: cesium cell

(θ, φ, z) of the beam on the fiber core and a power balancing in each of the three molasses beam pairs at 1% level. The slave diode laser current is 110 mA and the output power of the fibers exceeds 12 mW/fiber. Higher coupling efficiencies have been obtained (17 mW/fiber), but it is delicate to optimize the alignment for both the nominal and redundant diode lasers. Thus, the resulting laser power is a trade-off between the different laser configurations.

A second ECDL (with its backup ECDL) is locked to the cesium crossover resonance ($6S_{1/2}$, $F = 3 \rightarrow 6P_{3/2}$, $F = 3/F = 4$). The beam passes through a 101-MHz acousto-optic modulator (AOM5) and is split into four. Two beams are injected into optical fibers to repump the atoms during selection and detection. The two others are superimposed on the slave beams. All fixed-frequency AOMs (AA Opto-Electronic) have an optical efficiency better than 80% with a rf power of 150 mW. They are also used as actuators for the laser power servo loop and can switch off the laser beam intensity by 60 dB. In addition, five mechanical shutters ensure complete extinction of the beams (120 dB).

The integrated laser source is shown in Fig. 4. The optical components are mounted on a double-sided optical bench. The bench is fixed on the baseplate through four dampers and its first resonance frequency is above 150 Hz. The temperature regulation of the bench is ensured by a combination of heaters and Peltier coolers to maintain the temperature at 26 °C when the baseplate temperature varies from 10 to 35 °C. The electronics package is fixed to the baseplate. It includes all the laser source drivers. The laser source functions and the laser beam noise levels (frequency and power) have been verified under air and vacuum conditions in the 10–35 °C temperature range. The laser beams are guided toward the cesium tube by 10 polarization-maintaining fibers. Ten connectors with insertion loss of 1 dB ensure the link with the cesium tube fibers.

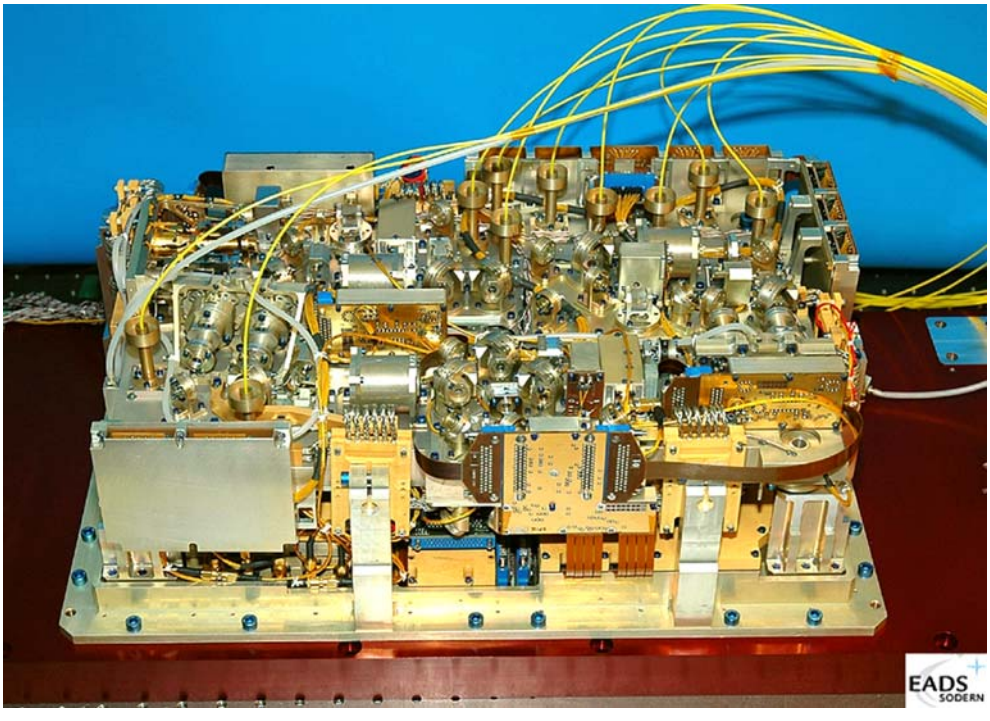

FIGURE 4 Photograph of the integrated laser source with cover removed. The dimensions are $530 \times 350 \times 150\,\text{mm}^3$ and the mass is 20.054 kg. The 10 polarization-maintaining optical fibers in *yellow* guide the laser beams to the cesium tube. All diode lasers (JDSU) are mounted on a Peltier cooler for temperature regulation within 2 mK (courtesy EADS SODERN)

3 The cesium tube

The second PHARAO instrument sub-system is the chamber in which the cesium atoms are cooled and state selected, interact with the microwave field, and are detected (Fig. 5). The total mass is 44 kg and the power dissipation is 6 W. A cylindrical vacuum chamber about 80-cm long is closed by a cesium reservoir on one side and by a 2-l/s ion pump on the other side. The reservoir is filled with 3 g of cesium. The cesium flux is regulated by the reservoir temperature (40–60 °C) and a motorized valve. To retain the liquid cesium within the reservoir chamber, a titanium foam covers the reservoir surfaces. A cesium vapor is produced in the capture zone where the six cooling laser beams are expanded to a waist of 5.5 mm (the optical molasses beam size is 26 mm truncated by the window). The beam polarization configuration is lin $\perp$ lin. Between the output port of the fiber and the beam collimator mounted tightly on the vacuum chamber a polarizing beam splitter reflects the counterpropagating beam towards a photodiode to monitor and lock the laser beam power. A photodiode mounted on a window collects the fluorescence of atoms in the vapor as well as atoms captured in the optical molasses.

By using a probe laser beam, we have measured the variation of the cesium pressure as a function of the valve aperture and the reservoir temperature. The results show that the vapor Cs pressure can be adjusted from 2×10^{-8} to 10^{-5} Pa. This range covers all utilizations: low vapor pressure to verify the residual vacuum level and measure diffusive losses out of the optical molasses as well as high vapor pressure to reduce the cold atom loading time.

A TE_{001} microwave preparation cavity with cut-off aperture of 8×9 mm closes the capture zone. The microwave field induces a selective transition between a single Zeeman sub-level of the two hyperfine levels ($F = 4, m_F = 0 \rightarrow F = 3, m_F = 0$ for clock operation, $F = 4, m_F \neq 0 \rightarrow F = 3, m_F$ for magnetic field evaluation). At the output a first laser beam induces a transition from $F = 3$ to $F = 4$ of the D_2 line. It is followed by a second laser beam tuned to the $F = 4$, $F = 5$ transition to push away the atoms in the $F = 4$ hyperfine level. This beam lets the atoms in the $F = 3$ state pass through. By pulsing the first beam, the $F = 3$ atom cloud can be sliced to study the atomic spatial distribution.

The interrogation zone bears a Ramsey cavity 20-cm long with 30-mm cut-off waveguides. The performances of the cavity flight model have been verified inside the LNE-SYRTE fountain FO1 [5]. No frequency shift (phase distribution, magnetic anomaly, and microwave leakage) appears at the experimental resolution level of 4×10^{-16}. As the cavity-induced phase shift is proportional to the atomic velocity, we will re-evaluate this effect in microgravity thanks to the new physical variable: the atomic velocity which can be changed over two orders of magnitude.

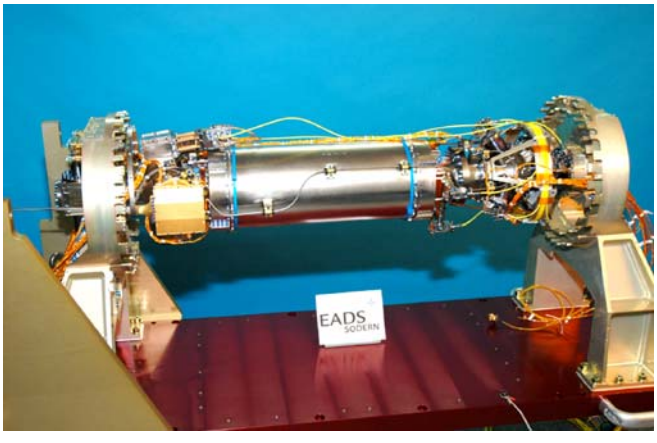

FIGURE 5 The integrated cesium tube without the two external magnetic shields. The volume is $990 \times 336 \times 444$ mm^3 and the total mass is 44 kg

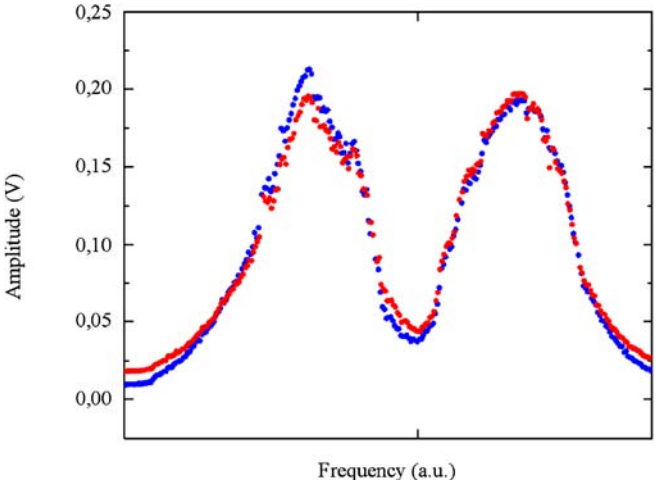

FIGURE 6 Fluorescence signals radiated by the residual thermal beam inside the two detection beams (*red and blue points*) as a function of the laser frequency. The standing waves are tilted with respect to the atomic beam. The fluorescence signals are split into two maxima (separated by 80 MHz) on both sides of the central frequency corresponding to zero-velocity atoms. When the laser beam is tuned to the central frequency to optimize the slow atom ($V < 5$ m/s) fluorescence signal, the thermal beam contribution is decreased by a factor of 10 at low saturation. For this test we have used a commercial Distributed Bragg Reflector (DBR) laser whose corresponding frequency noise appears on the fluorescence peaks

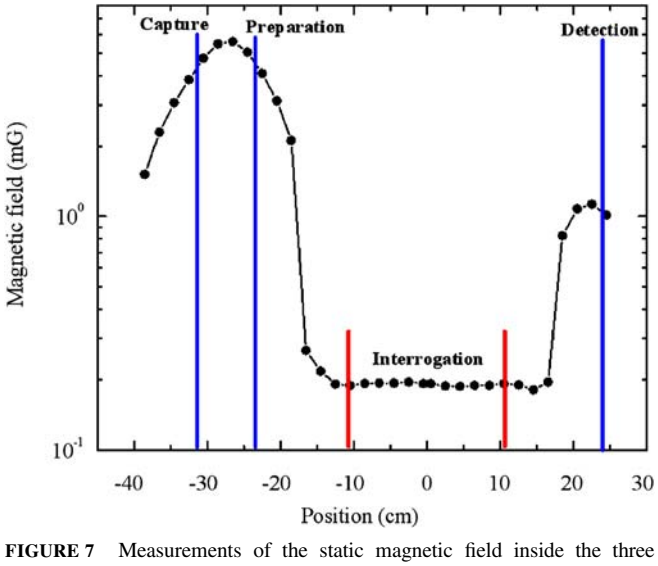

FIGURE 7 Measurements of the static magnetic field inside the three shields along the atomic path. The *lines* indicate the positions of the different zones. The interrogation zone is defined by the *red lines*

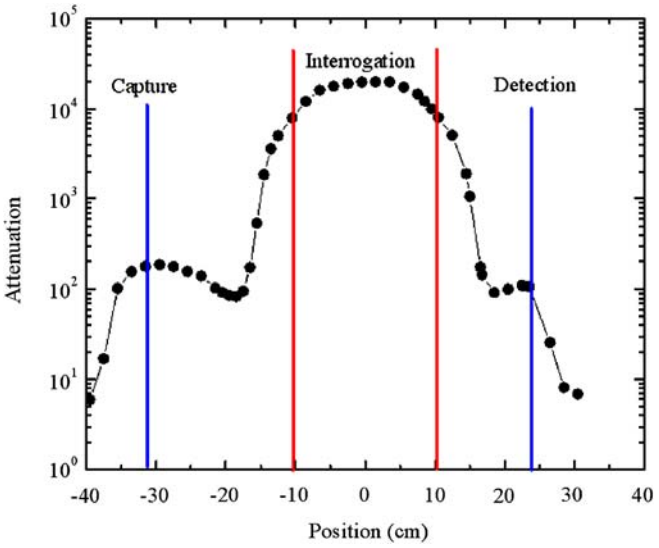

FIGURE 8 Measurements of the magnetic attenuation along the atomic path

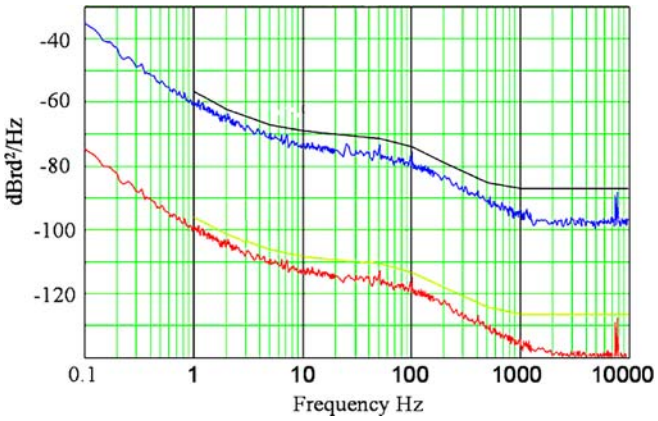

FIGURE 9 The measured phase noise of the microwave source at 100 MHz (in *red*) and at 9.2 GHz (in *blue*). The *continuous lines* indicate the PHARAO specification levels

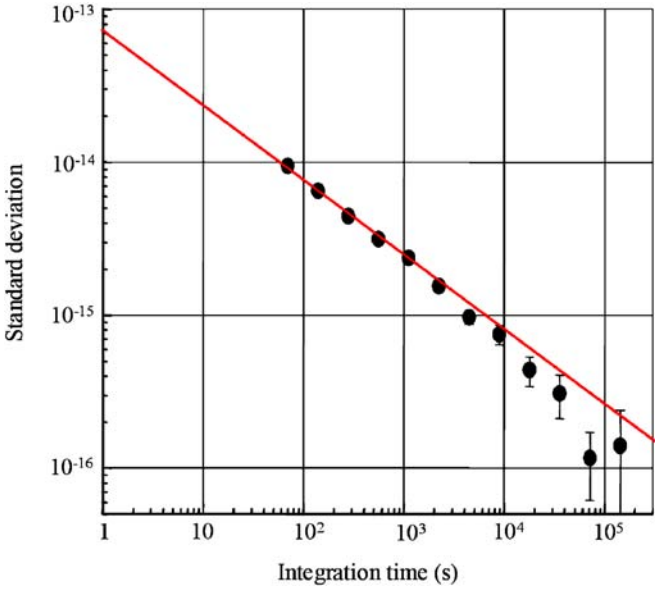

FIGURE 10 Test of the PHARAO microwave source: frequency stability of the LNE-SYRTE cesium fountain FO2 when it is driven by the microwave source. The *red line* is $7 \times 10^{-14}\ \tau^{-1/2}$. With the cryogenic oscillator the FO2 frequency stability is $1.6 \times 10^{-14}\ \tau^{-1/2}$

To improve the vacuum level in this interrogation zone and reduce collisions with thermal atoms, five getters are distributed on the internal side of the vacuum chamber. Furthermore, graphite getters prevent cesium migration from the capture region to the others.

Finally, the cold atom cloud enters the detection zone. It successively passes through four laser beams tilted by 8° with respect to the atoms' propagation direction. The first and fourth are standing waves with circular polarization tuned to the cesium D_2 $F = 4$, $F = 5$ cycling transition. They induce fluorescence signals which are collected by two condensers with an efficiency of 5%. The two photodiode signals are digitized by the computer to calculate the transition probability. The second beam tuned to the $F = 4$, $F = 5$ transition is a traveling wave to push away atoms in the $F = 4$ level after their detection. The third beam tuned to the $F = 3$, $F = 4$ transition pumps the $F = 3$ atoms to the $F = 4$ level. These atoms are subsequently detected by the fourth standing wave laser beam. As the beams are tilted, the residual thermal cesium beam which escapes from the capture zone is off resonance by 40 MHz. The stray fluorescence emitted by this fast beam is then reduced by at least a factor of 10 (Fig. 6) and it reaches the same very low level as the residual stray light. Their noise contributions to the detected atomic signal is then negligible in usual operation. The photodetection has a transfer gain of 15 V for 1 μW radiated by the atoms and the noise level is $4\ \mu V/\sqrt{Hz}$ in the 1–100 Hz frequency band.

The vacuum level deduced from the calibrated ion pump current is 2×10^{-7} Pa and decreased to 10^{-8} Pa when the cesium tube is under vacuum. A vacuum level of 2×10^{-8} Pa is required to limit thermal collisions when the lowest atomic velocity is studied in microgravity.

A magnetic shield with a solenoid and compensation coils at both ends surrounds the interrogation zone to define the clock bias magnetic field. A second magnetic shield encloses the vacuum chamber from the capture zone to the detection zone. Two inner coils define the magnetic field in the preparation cavity and the detection zone. Compensation coils are also positioned close to the first magnetic shield apertures to improve the magnetic homogeneity. A coil wound around the second shield with a magnetic probe compensates the fluctuations of the external magnetic field. Finally, a third magnetic shield encloses the whole device. Figure 7 shows the experimental measurements of the static magnetic field in a typical configuration. In the interrogation zone, the inhomogeneity is lower than 10 μG. This level is compatible with 10^{-16} clock accuracy. The magnetic field attenuation has been measured by using Helmholtz coils of 2-m diameter fed by a slowly oscillating (10-mHz) current. The coils supply a 400-mG magnetic field to simulate the variations on board the International Space Station orbiting the Earth. The resulting passive attenuation is shown in Fig. 8.

In the interrogation zone, the attenuation is 2×10^4. We have also tested a simple proportional digital servo loop by using the active compensation coil and the magnetic probe. The measurements have shown an attenuation of about

3×10^5 inside the interrogation zone limited by the hysteresis cycle of the shields. This attenuation will lead to 10^{-16} frequency variations on board the International Space Station. This level has still to be improved by a factor of five in order to practically neglect the magnetic field effect in the frequency accuracy budget of the clock. Either we will take into account the different behaviors of the hysteresis cycles of the shields to improve the digital servo loop or procure better magnetic shields. Some measurements made on a mock-up similar to the EM magnetic shields (but with different chemical composition) have demonstrated a static attenuation of 10^5, which guarantees the requirement.

Finally, we have tested the demagnetization process. A single wire passes through the magnetic shields to demagnetize them with a current of 2 A at a frequency of 0.1 Hz. Several tens of magnetization/demagnetization experiments show that the residual magnetic field is practically the same with a good symmetry in the interrogation zone. In addition, this field is easily compensated by the coils to obtain a field inhomogeneity below 10 μG.

4 The microwave source

The microwave source is based on the frequency multiplication of a very low phase noise quartz oscillator up to 9.192 GHz. The mass is 7 kg, the power dissipation is 21 W, and the dimensions are $300 \times 270 \times 177\ \text{mm}^3$. The quartz frequency (5 MHz) is multiplied and mixed with the signal of a direct digital synthesizer (DDS) to supply a 100-MHz signal. The DDS is mainly used to frequency lock (response time > 2 s) the 100-MHz signal to an external oscillator (the H maser of the ACES system). The purpose of this loop is to optimize at all Fourier frequencies the frequency noise spectrum of the 100-MHz signal.

The 100-MHz signal is multiplied and mixed with the signal of a second DDS, which drives the microwave frequency at 9.192 GHz. Two microwave signals are generated with independent amplitude and frequency: one for the preparation of atoms in a well-defined magnetic sub-state and the other for the microwave interrogation. As the frequency is defined by the same DDS, an external digital signal (PCP) switches between two DDS registers to quickly commute the frequency after the atoms leave the preparation cavity. This signal also switches off the preparation cavity microwave signal by 80 dB to ensure insignificant microwave leakage.

The phase noise spectral densities of the 100-MHz and 9.192-GHz signals are shown in Fig. 9. The noise level is mainly determined by the 5-MHz quartz oscillator phase noise; the contribution of the other elements is 10 dB lower. The microwave chain frequency stability has been measured against a sapphire cryogenic oscillator [7] at a level of 6×10^{-14} for time durations below 10 s. The microwave source has been extensively tested using the LNE-SYRTE FO2 atomic fountain. Using a cryogenic oscillator as interrogation oscillator and sufficient atom number, this fountain displays a frequency stability of $1.6 \times 10^{-14}\,\tau^{-1/2}$ [6]. With the PHARAO synthesis chain, weakly phase locked on the 100-MHz signal synthesized from the cryogenic oscillator signal, the frequency stability is $7 \times 10^{-14}\,\tau^{-1/2}$ as shown in Fig. 10. It is the best frequency stability ever achieved in a fountain with a quartz oscillator as interrogation oscillator.

FIGURE 11 The PHARAO space clock under test in CNES, Toulouse. On Earth the tube is set vertical. The laser source (on the *left*) is covered with a multilayer insulator. In this picture the chamber in which the vacuum tests are performed is opened. The clock can be operated both at atmospheric pressure and in vacuum

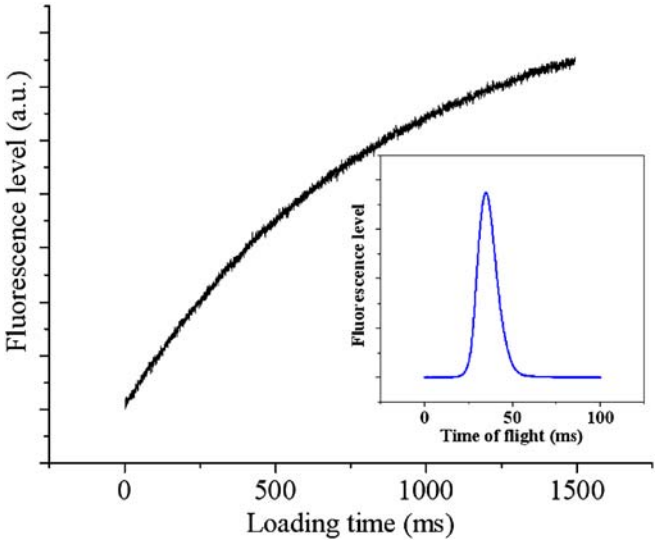

FIGURE 12 The fluorescence signal evolution during the atom capture. The time constant is 800 ms and the cesium pressure is 9×10^{-6} Pa. The *inset* is the detected time of flight signal when the atoms are launched upwards at a velocity of 3.4 m/s

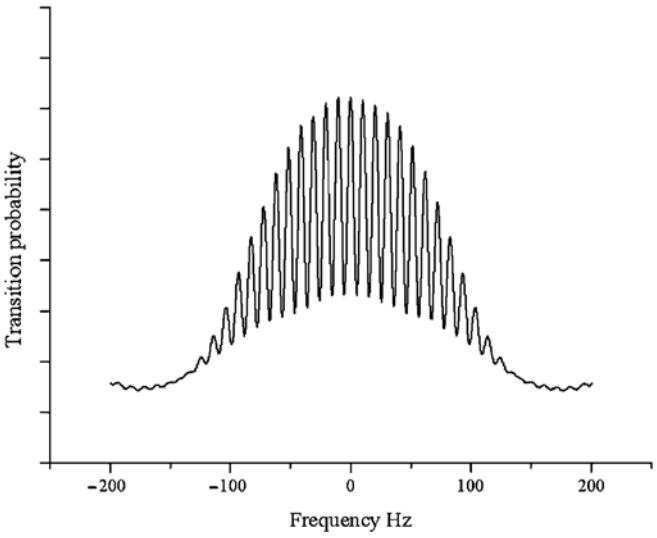

FIGURE 13 Transition probability as a function of the microwave field detuning around 9 192 631 770 Hz. For an upwards launch velocity of 3.4 m/s, the width of the central resonance is 5 Hz. Although the atomic selection in $m_F = 0$ was not used for this measurement, the signal to noise ratio reaches several hundreds

The microwave source has also been tested in a differential configuration by using a set of high-performance frequency synthesizers developed at the LNE-SYRTE in conjunction with the cryogenic sapphire oscillator. We have detected a small spurious 100-MHz transient phase pulse ($\simeq 10\,\mu$rad) synchronized with the PCP digital signal. As the 100-MHz signal is locked to the cryogenic oscillator through the DDS, this pulse is integrated by the phase-lock loop (response time $\simeq 1$ s), leading to a phase drift when the atoms are in the interrogation cavity. The measured resulting clock frequency shift is 6×10^{-16}, an unacceptable level for a target accuracy of 1×10^{-16}. This effect has been corrected and tested on the flight model of the microwave source. To cancel this effect on the PHARAO engineering model when it is locked to an external oscillator, we hold the phase lock loop error signal for the duration of the PCP signal, thus canceling the phase error on the microwave field seen by the atoms in the Ramsey cavity.

5 The computer

The computer controls the operation of the subsystems by three different RS422 lines. In addition, by using 23 digital lines the computer sends trigger signals to the sub-systems at different phases of the clock cycle, for instance the AOM frequency changes, the mechanical shutter operations, or the microwave source frequency. The computer also receives analog signals to be digitized and monitored. The main signals are the fluorescence signal in the capture zone as well as the detection fluorescence signals to measure the clock transition probability. The computer also implements other monitoring functions and servo loops, for instance the temperature regulations of the laser source and of the cesium tube as well as the magnetic field control. Finally, the computer is connected to the ACES payload through a RS422 line for data exchanges for TM/TC (telemetry/telecommand to be downloaded to the ground segment).

6 PHARAO first test results

In April 2006, in the CNES Toulouse PHARAO integration room, the laser source was connected to the cesium tube through optical fiber savers. Each sub-system was operated with its own ground-support equipment. The cesium tube was mounted vertically with the detection zone at the top as shown in Fig. 11. We have performed a preliminary study of the atomic capture, cooling, and launching. The atoms are launched upwards at a velocity of 3.4 m/s in order to reach the detection zone. Time of flight signals with excellent signal to noise ratio are obtained (see Fig. 12), indicating extremely low levels of stray light in the detection region and very good laser intensity and frequency stability. By integrating the time of flight signal over time we have deduced a number of detected atoms of 10^7, in accordance with the expectation from laser power and detuning in the cooling zone. As the apogee of the atoms is 5 cm higher than the detection beams, we have been able to detect the cloud when it returns to the detection zone in order to measure the temperature. We deduce a temperature of 2.5 μK, in agreement with expectations for cesium near molasses threshold at low intensity over detuning ratio [8]. Using the adiabatic cooling technique (the laser intensity after launch is reduced with a time constant of $\simeq 300\,\mu$s), the temperature will further reduce to 1 μK.

We have also connected a microwave source to the interrogation cavity and obtained the first PHARAO clock signal. The frequency scan near 9 192 631 770 Hz reveals the Ramsey fringes shown in Fig. 13. For a launch velocity of 3.42 m/s, the atoms spend 100 ms between the two Ramsey interactions and the fringe width is 5 Hz. The signal to noise ratio is several hundreds per cycle. The central pattern contrast is only 75%, as the atoms are decelerated by gravity and therefore do not undergo the same Rabi excitation in the two interaction sections.

7 Conclusion

In summary, these first performance tests have revealed a very satisfactory behavior of the cesium tube and laser source. The first PHARAO science run described in this paper has demonstrated the essential operations of a cold atom cesium clock designed for microgravity environment. The next steps involve tests of the flight software, atomic selection in magnetic sub-levels, adiabatic cooling to 1 μK, direct measurement with the cold atoms of the magnetic field and its stability versus temperature variations, microwave leakage, and cold collisions. These tests will be performed in thermal vacuum environment to be representative of the environment experienced by the PHARAO instrument on board the International Space Station. From August 2007, the PHARAO instrument will be tested together with the space hydrogen maser and the frequency-comparison device of the ACES payload. The goal of these performance evaluations is to reach a frequency accuracy of 10^{-15} on the ground, in order to safely anticipate an accuracy of 10^{-16} in space. The set of clocks of the ACES mission together with the ultra-stable time and frequency transfer system (MWL) opens new directions in fundamental physics research, navigation and positioning, and relativistic geodesy.

ACKNOWLEDGEMENTS The authors would like to acknowledge the industrial teams from EADS-SODERN, THALES, CMAC, EREMS, and CSSI which provided the various PHARAO sub-systems. We thank the members of the CNES technical support, Michel Aubourg from IRCOM for the simulations of the microwave cavity field, Sylvie Léon, and Richard Bonneville for continuous support. We acknowledge the ACES science team for numerous stimulating discussions. This work is supported by CNES, CNRS, LNE, and région Ile de France (IFRAF). The SYRTE is a unit associated with CNRS UMR 8630. The Laboratoire Kastler Brossel is a unit associated with CNRS UMR 8552 and with University Pierre and Marie Curie.

REFERENCES

1 C. Salomon, N. Dimarcq, M. Abgrall, A. Clairon, P. Laurent, P. Lemonde, G. Santarelli, P. Uhrich, L.G. Bernier, G. Busca, A. Jornod, P. Thomann, E. Samain, P. Wolf, F. Gonzalez, P. Guillemot, S. Leon, F. Nouel, C. Sirmain, S. Feltham, C.R. Acad. Sci. Paris IV **2**, 1313 (2001)

2 F. Allard, I. Maksimovic, M. Abgrall, P. Laurent, Rev. Sci. Instrum. **75**, 54 (2004)

3 X. Baillard, A. Gauguet, S. Bize, P. Lemonde, Ph. Laurent, A. Clairon, P. Rosenbusch, Opt. Commun. (2006), in press

4 A. Clairon, P. Laurent, G. Santarelli, S. Ghezali, S.N. Lea, M. Bahoura, IEEE Trans. Instrum. Meas. **44**, 128 (1995)

5 C. Vian, P. Rosenbush, H. Marion, S. Bize, L. Cacciapuoti, S. Zhang, M. Abgrall, D. Chambon, I. Maksimovic, P. Laurent, G. Santarelli, A. Clairon, A. Luiten, M. Tobar, C. Salomon, IEEE Trans. Instrum. Meas. **54**, 833 (2005)

6 S. Bize, Ph. Laurent, M. Abgrall, I. Maksimovic, L. Cacciapuoti, J. Grunert, C. Vian, F. Pereira Dos Santos, P. Rosenbush, P. Lemonde, G. Santarelli, P. Wolf, A. Clairon, A. Luiten, M. Tobar, C. Salomon, C.R. Physique **5**, 829 (2004)

7 A.G. Mann, S. Chang, A.N. Luiten, IEEE Trans. Instrum. Meas. **50**, 519 (2001)

8 C. Salomon, J. Dalibard, W.D. Phillips, A. Clairon, S. Guellati, Europhys. Lett. **12**, 683 (1990)